The Structure and Thermodynamics of an Intense Mesoscale Convective Storm in Oklahoma

FREDERICK SANDERS AND ROBERT J. PAINE[1]

Department of Meteorology, Massachusetts Institute of Technology, Cambridge 02139

(Manuscript received 10 February 1975, in revised form 22 April 1975)

ABSTRACT

On 14 May 1970 a cold front passed through the mesonetwork of the National Severe Storms Laboratory in central Oklahoma. As it did so, intense convection developed and thunderstorms produced more than 2 inches of rain at some points within the network. On this date a total of 58 rawinsonde observations were made at nine stations within the network, 42 of them during the period from about 1 h prior to frontal passage to 2 h afterward.

We have analyzed these as well as other data to arrive at a picture of the structure of the mesoscale system and of the thermodynamical processes operating in it. The front first encountered potentially unstable moist air as it passed through the network. As this air was lifted frontally the instability was released, with remarkable results. A mesoscale downdraft-updraft doublet developed in the warm air aloft, with peak speeds at 400 mb of 2–3 m s^{-1} over 10 km widths transverse to the front, the descent being above the surface frontal position and the ascent (which produced almost all the precipitation) being about 30 km toward the colder air to the northwest.

The downdraft appears to be driven by intense cooling due to evaporation of the initial deep cumulus clouds into the very dry air aloft. The updraft is due to condensational heating on the mesoscale, in saturated air of nearly neutral stability, with convective activity superimposed. We conjecture that these diabatic effects permit the mesoscale vertical motions to proceed for several hours without large perturbation of the isentropic surfaces. The character of the convection, and of the mesoscale circulation, is not accounted for by a simple model of an entraining convective plume.

We present evidence that the balloons tended on the average to be drawn into the convective-scale updrafts and to avoid the downdrafts, thus yielding spurious indications of the percentage of volume occupied by active convective updrafts and downdrafts. We find, on the other hand, that deviations of balloon ascent rate and equivalent-potential temperature of individual soundings from the means of their neighbors can be used to estimate convective transports. The virtual source of equivalent potential temperature, thus determined, is in reasonable agreement with the apparent source independently obtained as a residual in the mesoscale budget.

1. Introduction

Interaction of cumulus clouds with larger scales of motion represents one of the important unsolved problems of meteorology and has attracted lively interest in recent years. Most attention has been given to the effect of tropical convection upon the synoptic scales (Yanai *et al.*, 1973; Arakawa and Schubert, 1974; Ogura and Cho, 1973; Cho and Ogura, 1974). In higher latitudes, the organization of intense convection into mesoscale systems is a scientifically important process with vastly destructive consequences for the ecosphere, but the interaction between cumulus elements and mesoscale pattern has been studied relatively little (Nimomiya, 1971). A reason, no doubt, is that average effects on the synoptic scales can be elucidated with routinely available observations, but the mesoscale can be satisfactorily examined only with data from special networks. Such a network has been maintained for several years by the National Severe Storms Laboratory (NSSL) in Oklahoma, as described by Barnes *et al.* (1971).

The NSSL rawinsonde data has received little use. Lewis *et al.* (1974) have studied a case for which 21 soundings were available for the period of interest, but analyzed only the period immediately prior to the onset of severe convection. We selected the case of 14 May 1970, when 58 soundings were made, 42 during a 5 h period in which a cold front passed through the network accompanied by thunderstorms with heavy rainfall but few severe events, probably the most intensively observed case of this kind.

Our original goal was to study the interactions by determining how the mesoscale environment was modified by the convection so as to sustain the ever deeper clouds which developed as the system ap-

[1] Present affiliation: Environmental Research & Technology, Inc., Lexington, Mass.

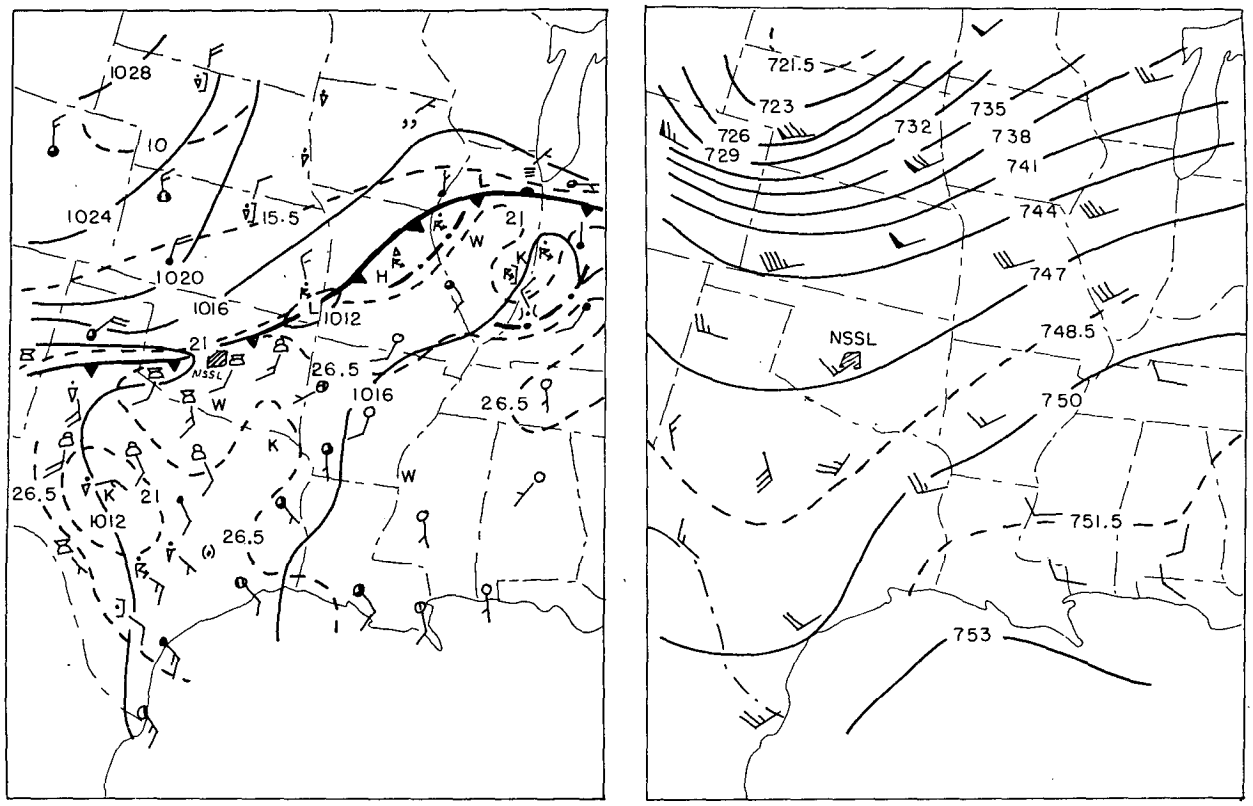

FIG. 1. Synoptic situation at 1800 CST 14 May 1970. Hatched area indicates location of NSSL mesonetwork. (a) Surface map. Solid lines are isobars (mb) of sea-level pressure; dashed lines are surface isotherms (°C). Letters L, W and K indicate, respectively, centers of low pressure and warm and cold temperature. Front, instability line, wind, cloud amount and present weather phenomena are indicated in standard synoptic notation. (b) 400 mb chart. Solid and dashed lines are height contours (decameters). Winds are indicated in standard synoptic notation.

proached and passed, using a simple convective plume model to measure the susceptibility of the atmosphere to convective overturning and to check the convective transports obtained as residuals in the mesoscale budgets. We had limited success in this, but in the process obtained a new and apparently self-consistent view of the physical nature of the storm as a whole. Details of the work have been given by Paine (1975).

2. The synoptic situation

The synoptic features at 1800 CST are shown in Fig. 1. In the surface analysis a cold front extended from northern Indiana and Illinois southwestward into New Mexico, as in the case studied by Lewis *et al.* (1974). This front was just entering the northwest corner of the NSSL network, progressing southeastward at a speed of about 24 km h^{-1}. Squall-line and air-mass thunderstorms were occurring far ahead of the front in the broad southeasterly flow from the Gulf of Mexico, but will not concern us.

The 400 mb analysis shows a pronounced short-wave trough in the upper Great Plains with a weak extension into western Oklahoma and Texas, rather different from the Lewis case.

3. Observations and organization of data

a. Surface observations

In 1970 the network included 44 automatically recording surface stations in a 70 km square in central Oklahoma. Each was equipped to measure wind direction and speed, temperature, relative humidity, pressure and rainfall.

A study of the surface wind reveals that an abrupt frontal wind-shift line progressed steadily through the network. Fig. 2 shows the distribution of surface stations and the advance of the line (hereafter denoted the SWS). A coordinate system moving with the front is shown in Fig. 2. The y axis, where use is made of it, passes through the NSSL radar site. Before the arrival of the SWS, the wind blew steadily from a direction between southeast and south-southwest. The frontal passage was marked by a decrease in wind speed, followed by a shift to a direction between northwest and northeast. This sequence occurred in a period of

from 1–3 min and was followed by moderate gusts and variations in wind direction. Widespread precipitation did not commence at the surface until 40–70 min after passage of the SWS. Total amounts at individual stations ranged from 0.04 inch in the north to 2.26 inches in the south, the rainfall growing in both intensity and duration as the system passed through the network.

Although this system might be regarded as a squall line because of the associated thunderstorm activity, there is evidence to support the view that a front separating two air masses passed through the network. After the wind shifted, no instance of a southerly component was observed. Temperatures fell monotonically from around 25°C to about 15°C. Moreover, there is no evidence that the SWS was the result of a downdraft-produced gust front, which often accompanies squall lines.

b. Radar observations

The 10 cm WSR-57 NSSL radar presents a PPI isoechocontoured display of the effective reflectivity factor Z_e at 10 dB intervals. A sequence of sweeps starts at 0° elevation, followed by an automatic increase of 1° or 2° with each successive sweep, to a maximum of 20°. The radar data for this case have been used to aid the analysis of surface rainfall and relative humidity aloft, to provide estimates of cloud-top height, and to aid in interpretation of the character of the convective elements.

c. Rawinsonde data

In accordance with NSSL project requirements, tracking of rawinsondes was terminated at or slightly above the 400 mb level during the 3 h of greatest interest, in order to maximize the number of launches. Earlier and later the soundings reached 250 mb.

While the data coverage is impressive by ordinary standards, it is still far from sufficiently dense to be used in resolving the effects of individual convective cells in all three spatial dimensions and time, and is only marginally adequate for conventional mesoscale analysis at fixed times. However, the organization of the storm system into a well-defined line, and the short time span of the observational period, suggest preparation of a composite analysis based on the assumptions of a steady state and of no variation in the direction parallel to the SWS. Therefore, we analyzed the variables most carefully, and presented the results most completely, in a vertical plane transverse to the SWS. Rough measurements of variations along the x axis and in time, used in the budget calculations, generally confirm the validity of these assumptions.

Smoothing techniques were used to suppress unwanted details of vertical structure, in a manner similar to that of Fankhauser (1969). Thin layers in individual soundings which displayed highly unlikely equivalent

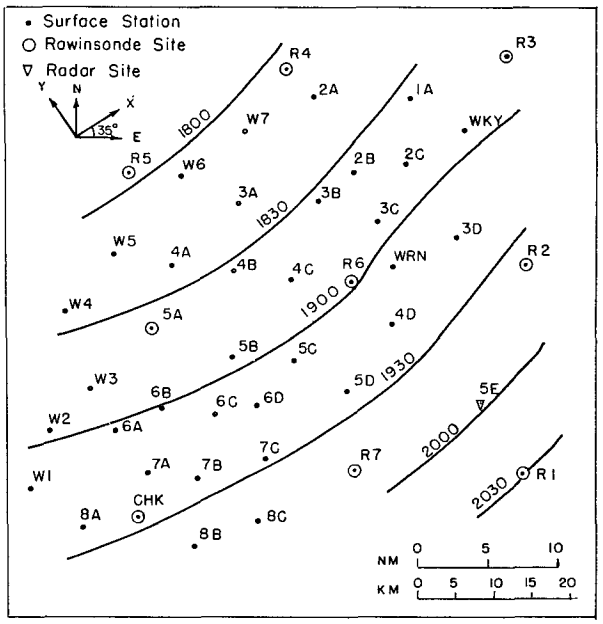

FIG. 2. Isochrones (CST) of surface wind shift. Dots represent stations of the mesonetwork. The coordinate system is indicated in the upper-left corner.

potential temperatures were corrected and the data were then averaged vertically in 50 mb layers. A horizontal running mean of meteorological quantities was obtained by averaging data from about ten balloons for each layer, then attributing that average value to the centroid of the balloon positions (which had been adjusted for change of time and location relative to launch). An overbar will be used to denote such averages.

The distribution of the vertically averaged data in the y-p plane is shown in Fig. 3. (At several points two or three balloons are superposed.) Note that the abscissa is labelled in terms of both time and distance relative to the SWS. The horizontal averaging scheme is illustrated for the layer centered at 725 mb by seven groups of circled data points. The resulting seven columns of horizontal centroids of balloon groups are also shown.

Derivatives of any quantity with respect to y and p were calculated by finite differences with mesh lengths of 8 km and 50 mb, respectively. Values at this array of points were obtained from the values at balloon centroids by subjective analysis. Derivatives in the x direction were estimated by dividing the balloons into two equal groups by means of a line parallel to the y axis, for each time block and pressure layer. An average value was calculated for each group of about five observations and was assigned to the centroid of the positions. Analysis and finite-differencing followed, with a mesh length of about 40 km. Local changes with respect to time were similarly estimated by treating each third of the relative time range. Within each third,

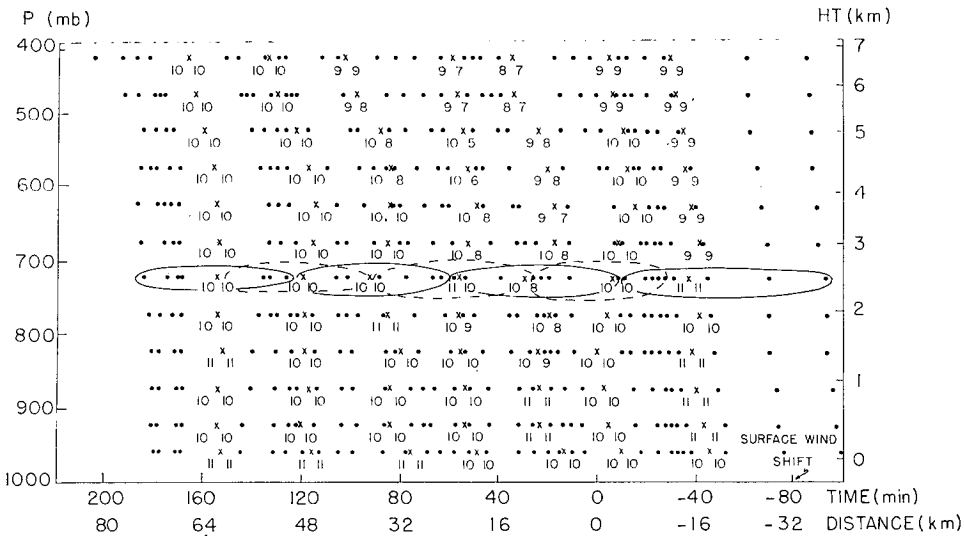

FIG. 3. Location of balloon data in the y-p plane. Dots represent positions of individual balloons at the surface and at 50 mb intervals. X's are positions of centroid of balloon groups. Numbers to the left and right of each centroid are the number of balloons which contributed, respectively to the Version A and Version B group means. See text, Section 4a. The grouping scheme is illustrated at 725 mb.

an average was computed for the earliest and latest halves of the observations on the basis of the CST observation time. Differences over a period of about 2 h were obtained in this way.

Fankhauser (1969) advised that releases of balloons into convective storms should be avoided because of possible equipment failure and the inability to resolve scales of motion associated with convective cells. In 1970, however, the rawinsonde observers attempted to launch balloons into active cells, though we have no information on the explicit strategy employed in this case.

Evidence that a number of balloons entered updrafts (and survived) during the 14 May storm is presented in the next section. A number of crashes occurred, however, from which only part of the data could be used. In any event, the compositing of the data which was permitted by this storm increases the density of the data sufficiently that the mesoscale pattern can be obtained with considerable confidence, and sufficiently that the individual soundings can provide a qualitatively reasonable estimate of the effect of the convective elements on this pattern, as we shall see.

In the vicinity of the intense convection, individual observed values may deviate strongly from the mean for the time block. To deal with extreme measurements that might have an undue effect on the arithmetic mean, we chose to apply a nonparametric algorithm, the "best easy systematic estimator" (Wonnacott and Wonnacott, 1972). The observations in a sample are sorted in numerical order, one-quarter of the values are discarded from each end of the list, and the average of the two remaining end values and the two middle values is obtained.

4. Distribution of the meteorological variables

a. Identification of convective and environmental soundings

In this study the properties of the mean mesoscale atmosphere are examined. In contrast to studies which consider the synoptic scale, ours cannot proceed on the *a priori* assumption that the properties of the mean are those of the convective environment, since it is possible that some of our mesoscale elements of volume may contain a substantial fraction of convective clouds. On the other hand, to make plume-model calculations we must have the properties of the environment alone. In either case, it is necessary to determine the extent to which individual soundings passed through convective clouds. To do this we must try to determine the vertical motion of the air in which the balloon rose, as the difference between the observed ascent rate and a hypothetical rate through a resting atmosphere.

Two methods were used to find the still-air ascent rate. One is theoretical while the other relies on observed pre-frontal ascent rates of balloons launched in this case at least 1 h before the arrival of the SWS, when the vertical motion of the air was presumably slight. Details are discussed in the Appendix. In short, both theory and our observations indicated that the ascent rate of the balloons increased from about 6 m s^{-1} at release to about 7 m s^{-1} at 400 mb.

For individual balloons throughout the entire area of analysis, the still-air ascent rate was assumed to be the actual ascent rate in the lowest 200 m. In most cases this rate was between 5.5 and 6.5 m s^{-1}. In precipitation areas, where the initial ascent rate was found in some cases to be less than 5.5 m s^{-1}, the still-air rate was

assumed to increase by 1 m s^{-1} from ground level to 400 mb.

In addition to these measurements, the equivalent potential temperature θ_E was used to identify convective soundings. Updrafts were assumed to be characterized by mean vertical motion exceeding 4 m s^{-1} in at least two 50 mb layers, accompanied by θ_E values in excess of the time-block mean by at least 3 K. Very seldom was only one requirement satisfied. Downdrafts were similarly identified by descent rate in excess of 2 m s^{-1}, accompanied by θ_E values at least 3 K lower than the block mean. In several instances, rapid descent of the balloon occurred without a deficit of θ_E, presumably because of heavy precipitation or ice load.

FIG. 4 is an x-y plot of the horizontal projection of the paths of the 42 rawinsonde balloons, relative to the moving front. Convective currents and instances of precipitation or icing are identified as explained above. An interesting feature is the location of identified convective currents. Most of the updrafts were located a few kilometers ahead of the echoes at the ground, while downdrafts and surface precipitation were found to the rear of the most intense echos.

Outflow beneath a downdraft will tend to deflect a balloon away, while inflow beneath an updraft will tend to attract the rising balloon. Thus the samples of balloons may tend to represent unrealistically large proportions of updrafts. Paine (1975) has shown on the basis of the kinematics of convective circulations that such a possibility cannot be discounted *a priori* in our case. We will see later strong indirect evidence that such bias was present. Moreover, as mentioned above, there may have been a conscious effort by the observers to launch balloons into updrafts, which, if successful, would have introduced a bias into the results, for the use we wish to make of them.

Because of uncertainty in the fraction of volume composed of updrafts (and since the properties of downdrafts in fact varied relatively little from those of their block means), we will present two displays of each meteorological quantity, denoted Version A and Version B. The first assumes no bias in the balloon sampling and initially accepts all observations. In Version B the updrafts are considered to occupy about 10% of the mesoscale volume element. Downdrafts are retained in both versions. Version B will be used for plume calculations, on the basis that in this case the mean can be identified with the environment without serious error.

b. "Meridional" wind component

As a matter of convenience, we will denote the component of wind along the y axis the "meridional" component, though it is directed toward the geographical direction 325°. Both Versions A and B of this component are shown in Fig. 5, in a fixed coordinate system. Note in both cases the strong gradient near the SWS at the surface and the maximum near 650 mb at

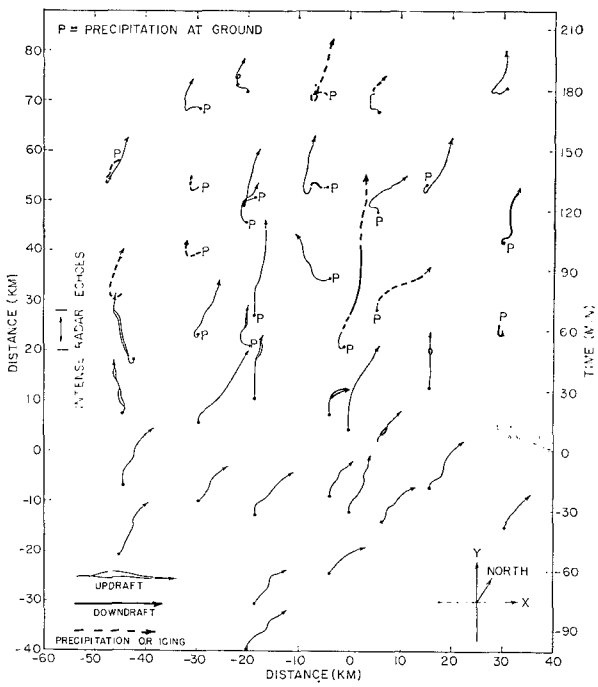

FIG. 4. Horizontal projection of trajectories of individual balloons moving relative to the surface wind-shift line.

+50 min, with minima on either side. These features do not represent geostrophic effects, since measurements show that the mesoscale gradient along the front, $\partial\bar{T}/\partial x$, is small and in fact negative at most points, inconsistent with the observed shear.

A comparison of the two versions implies that meridional components were larger, on the average, in updrafts than in the environment. Below 650 mb this finding is inconsistent with the hypothesis that the horizontal momentum of cloud air tends to be conserved as it rises, a notion which underlies much of our intuitive thinking.

An interesting feature is the vertical fluctuation in the sign of the meridional component near −40 min. This structure is remarkably consistent from sounding to sounding and is found far ahead of the SWS. It may represent the effects of gravity-wave activity spreading ahead of the intense storm to the northwest, as suggested by Lindzen.[2]

c. Vertical motion

The vertical motion can be calculated from the principal of continuity of mass by the traditional kinematic technique. Thus,

$$\bar{\omega}(p)=\bar{\omega}_s+\int_p^{p_s}\left(\frac{\partial\bar{u}}{\partial x}+\frac{\partial\bar{v}}{\partial y}\right)dp, \qquad (1)$$

[2] R. S. Lindzen, Harvard University, private communication.

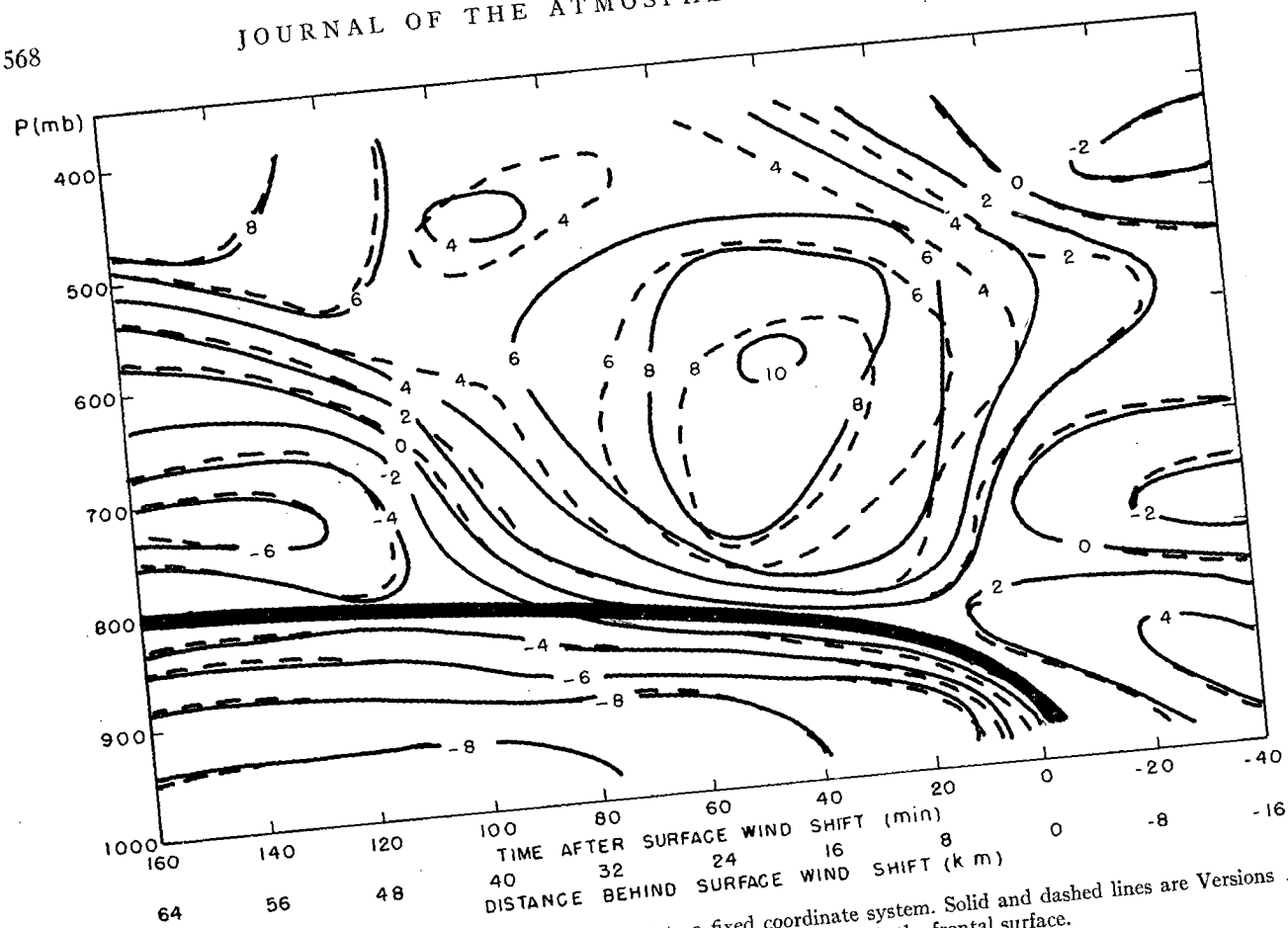

FIG. 5. "Meridional" components of wind (m s^{-1}) with respect to a fixed coordinate system. Solid and dashed lines are Versions A and B of the analysis, respectively. See text. Heavy solid line is the frontal surface.

where the subscript s refers to the earth's surface. Values of $\bar{\omega}$ are converted to values of $\bar{w}$ by the approximation, $\bar{w}=\bar{\omega}/(g\bar{\rho})$.

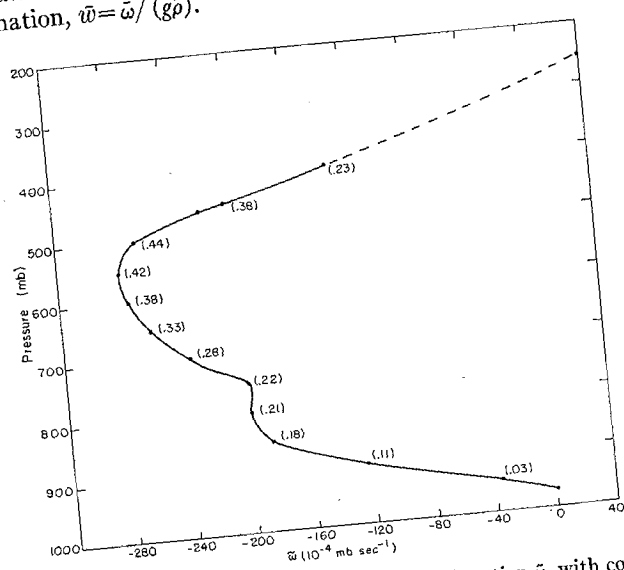

FIG. 6. Profile of domain-averaged vertical motion $\bar{\omega}$, with corresponding values of $\bar{w}$ (m s^{-1}) in parentheses. Dashed portion of profile is estimate based on relatively few data.

To get an idea of the overall pattern, we first calculated $\bar{\omega}$, the average vertical motion over the domain from -16 km to $+64$ km by the approximation

$$\bar{\omega}(p)=\frac{1}{80\text{ km}}\int_{p}^{p_s}[\bar{v}_{+64}(p)-\bar{v}_{-16}(p)]dp.$$

The result appears in Fig. 6. Vigorous ascent over this small synoptic-scale (or large mesoscale) volume reached a maximum in the layer from 600 to 500 mb and was decreasing sharply at 400 mb, the upper limit of intensive observation. The pattern is entirely credible and, so far as we can tell, does not suffer from the frequently encountered tendency of the kinematic method to yield spurious divergences over deep layers. Crude estimates based on higher soundings just outside the lateral limits of Fig. 5 indicate, in fact, that the ascent had entirely vanished slightly below the 250 mb level, the approximate level of the highest tops of radar echoes.

The irregularity in the profile near 800 mb is probably real. Reference to Fig. 5 shows that the strong convergence below this level is due to the frontal wind shift near the surface. The frontal surface, to judge from negative values and strong vertical shear of the com-

ponent of wind along the x axis (not shown), reaches the 800 mb level near +64 km, yielding a reasonable mean slope of about 1:30. The additional convergence in the layer from 750 to 550 mb, which gives the vertical motion a second boost, so to speak, is associated with the strong negative meridional components in the warm air aloft in the most northwestern 20 km of the analysis domain. This portion of the overall updraft is due, we believe, to the massive condensational heating triggered by the frontal lifting of potentially unstable air.

In the detailed calculation of the field of the mesoscale average $\bar{\omega}$, $\partial\bar{u}/\partial x$ was taken into account, however crudely, and the analyzed values of $\partial\bar{v}/\partial y$ were corrected to account for a small bias due to secular increase of $\bar{v}$ with time over the entire area, coupled with an earlier mean CST observation time in the northwestern than in the southeastern portion of the diagram. These effects contributed a value of $\bar{w}$ which was typically of the order of 0.1 m s^{-1} but reached a point maximum of 0.4 m s^{-1} at 400 mb. The value of $\bar{\omega}_s$ was relatively small throughout and was ignored in the calculations.

The detailed patterns based on both of the meridional-component analyses are shown in Figs. 7 and 8. A sloping band of ascent overlies the frontal surface up to the 750 mb level, above which a pronounced doublet of ascent and descent dominates the picture, both of which are related to the pronounced maximum in the meridional component discussed earlier (c.f. Fig. 5). Mesoscale vertical motions of more than 2 m s^{-1} occur over distances of about 10 km in both the updraft and the downdraft areas. The maximum vertical motions at 400 mb are about 0.5 m s^{-1} weaker in Version B than in Version A.

This pattern was so striking, and the downdraft so unexpected, that we undertook to confirm it by an investigation of the balloon ascent rates. An analysis of the Version A excess of mean ascent rate over the adopted values described earlier appears in Fig. 7. The correlation between two patterns is approximately zero, an inevitable result of the aforementioned coincidence of large meridional components with strong balloon ascent rates.

Version B of the balloon-determined vertical motions shows much better agreement, as can be seen in Fig. 8, with the zero isopleth aloft between 20 and 40 min after the SWS in both instances. In the ascent region, discrepancies exceed 0.5 m s^{-1} above the 450 mb level in general, and above the 700 mb level in particular between +100 and +140 min. In both these locations it is reasonable to conclude that heavy precipitation or accumulated load of snow and ice was slowing the ascent of the balloons. In the kinematical descent region, however, the balloons showed only slight descent, less than 0.5 m s^{-1}. Part of this discrepancy may be due to the criterion for identification of balloon updrafts, which relied on the assumption of relatively small mesoscale vertical motion in the environment of the convective elements. Had more balloons been identified as updraft cases in the region of kinematical descent, the two methods of obtaining vertical motions would have been in still better agreement in Version B.

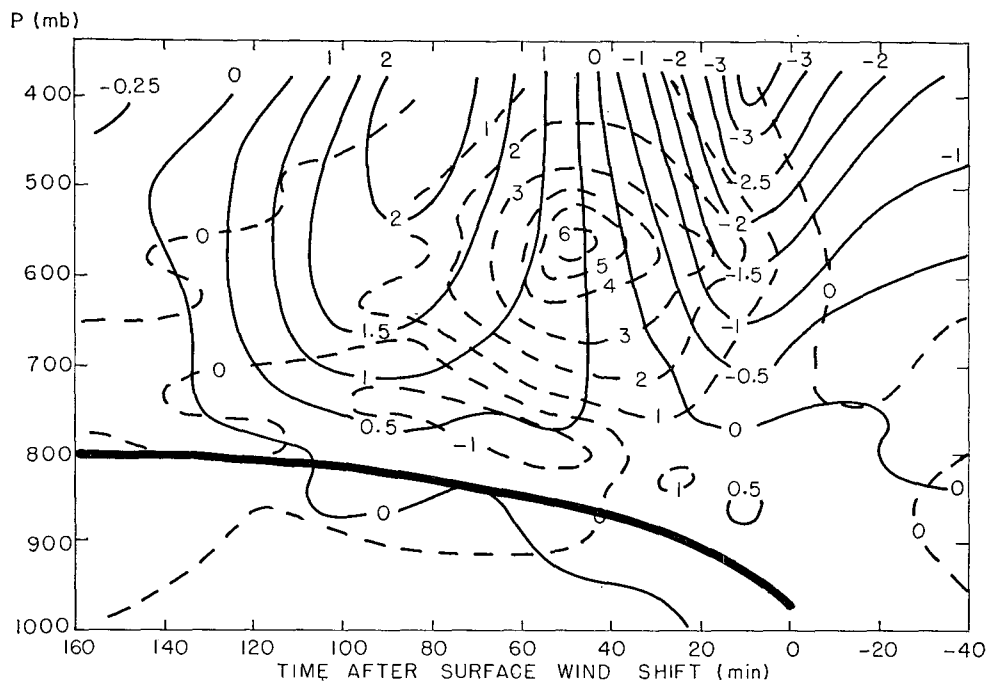

FIG. 7. Mesoscale vertical motions $\bar{w}$ (m s^{-1}) for Version A of the analysis. Solid lines are from conventional kinematic technique. Dashed lines are derived from balloon ascent rates.

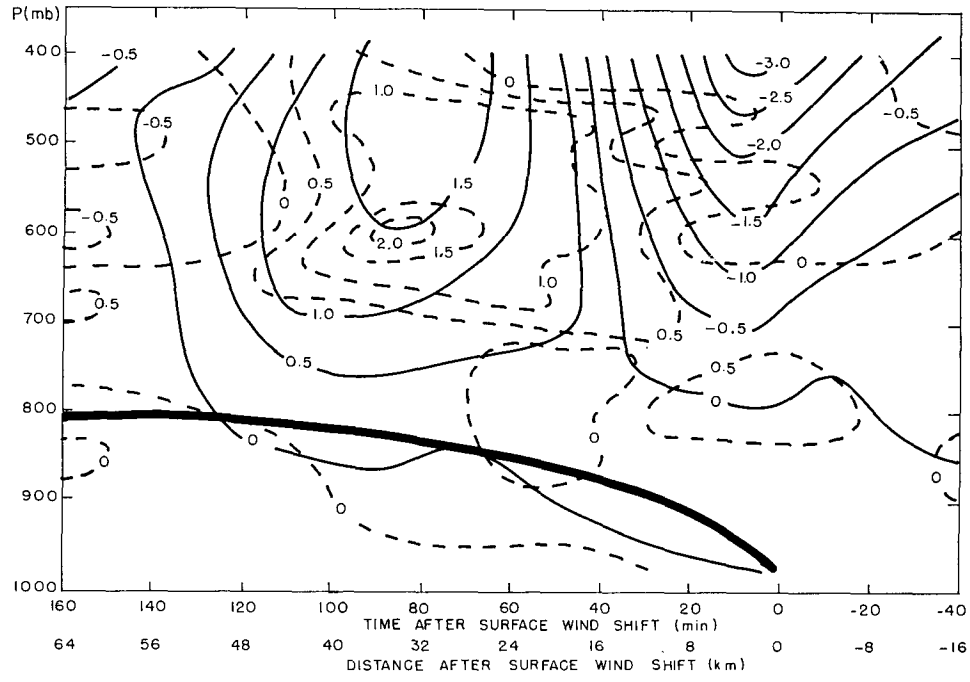

FIG. 8. As in Fig. 7 except for Version B.

Of course, all the Version B analyses were predicated on the assumption that only a small percentage of the mesoscale volume element was occupied by convective updrafts. As a test of this assumption we considered the hypothesis that the Version A pattern of balloon-derived vertical motions was in fact correct and used the equation of continuity in the approximate form

$$\bar{v}(y)=\bar{v}(-16\text{ km})-\int_{-16\text{ km}}^{y}\frac{\partial\bar{\omega}}{\partial p}dy,$$

to compute the $\bar{v}$ field, taking $\bar{\omega}$ from the balloon measurements and using the observed $\bar{v}$ values at the quiescent southeastern edge of the analysis domain. The results of this unconventional application of the kinematic method were absurd, with inflow and outflow speeds in excess of 70 and 60 m s^{-1} at and beyond +100 min near 725 and 525 mb, an order of magnitude larger than the observed values.

Consequently, we concluded that the balloons, whether by strategic design or otherwise, were in updrafts in an unrepresentative number of instances, and that the mesoscale vertical motions were not generally obtainable from the balloon ascent rates, even outside regions of precipitation. Therefore, we decided to rely on the kinematical vertical motions obtained from the observed horizontal components of motion, though not without some reservation.

d. Equivalent potential temperature

The field of equivalent potential temperature (Version B) is shown in Fig. 9. A tongue of high values extends upward and northwestward from the ground ahead of the SWS. From the axis of the tongue, as in the case studied by Lewis *et al.* (1974), $\bar{\theta}_E$ decreases upward (indicating potential instability) to a minimum near 550 mb ahead of the SWS and near 700 mb well to its rear. This minimum extends across the entire section, including the region of most active convection and heaviest rainfall, though it is weakest there. Above the minimum, $\bar{\theta}_E$ increases with height. In Version A, there is no qualitative difference in the pattern, but values are 2–3 K higher above the 800 mb level in the region of vigorous convection between +40 and +60 min. The minimum persists, however, near the 600 mb level.

Above the shallow wedge of cold air extending northwestward from the SWS, the relative air motion is generally upward and from right to left. However the details may be arranged, it is clear that $\bar{\theta}_E$ is not conserved in many places, following the mesoscale flow. In the lower portions of the warm air mass $\bar{\theta}_E$ is higher where air enters the section than where it leaves; at higher levels the opposite occurs. Thus, the smaller scale convective motions transfer $\bar{\theta}_E$ upward in the potentially unstable air mass, in accord with our intuitive notions. This matter is discussed in some detail in the following section.

e. Potential temperature

The Version B field of potential temperature appears in Fig. 10. The frontal surface is nearly parallel to the isentropic surfaces, running from 27°C at the ground to

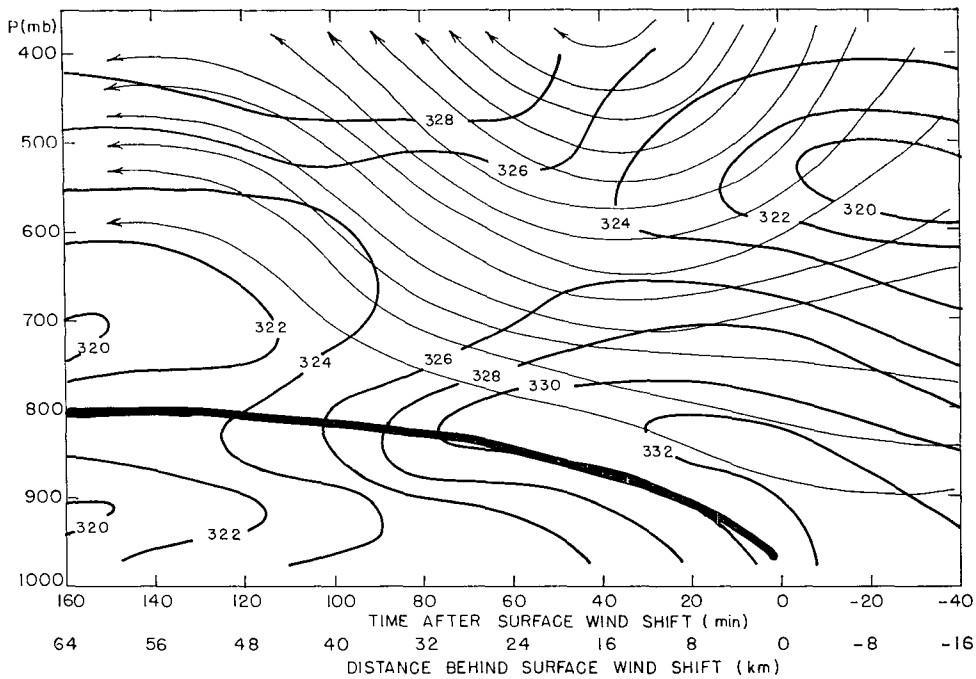

FIG. 9. Mesoscale equivalent potential temperature $\bar{\theta}_E$ (K) for Version B of the analysis, with streamfunction lines of flow relative to the surface wind-shift line, from Version A. Latter are at intervals of 500 mb m s^{-1}, with direction of flow shown by arrow heads.

28°C at 800 mb, but is not accompanied by a marked stable layer. Within the warm air, potential temperature decreases northwestward up to about 550 mb, above which the horizontal gradient is reversed. The Version A analysis differs by no more than 1°C at any point.

The air, on the average, is heated as it moves upward

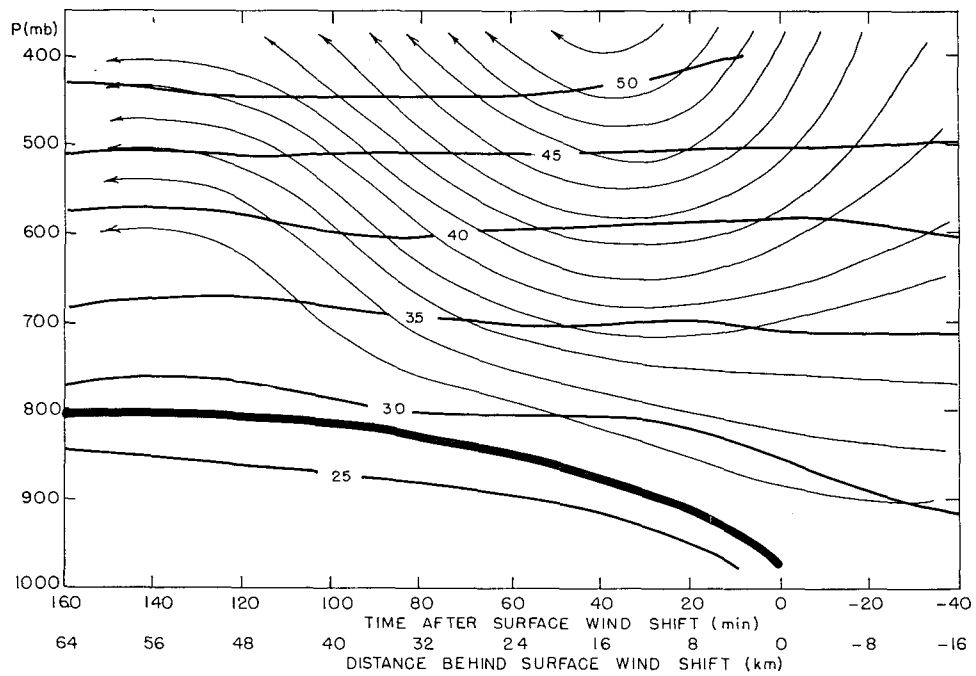

FIG. 10. Mesoscale potential temperature $\bar{\theta}$ (°C), for Version B of the analysis. Streamfunction lines are as in Fig. 9.

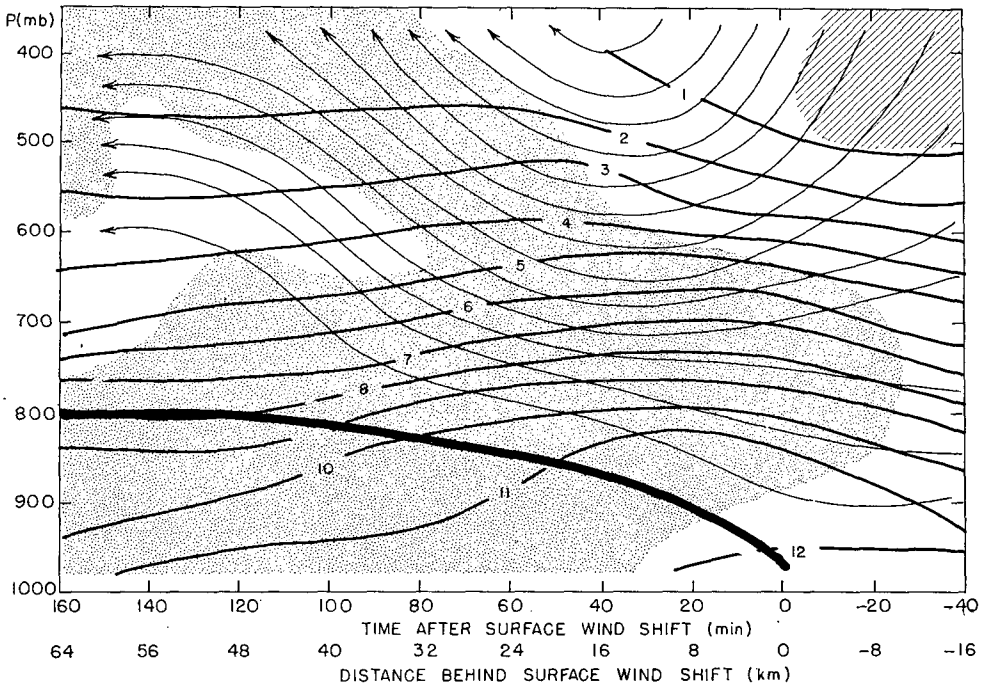

FIG. 11. Mesoscale mixing ratio $\bar{r}$, labelled in units of 10^{-3}, for Version B of the analysis. Streamfunction lines are as in Fig. 9. Hatching and stippling represent, respectively, areas of relative humidity less than 25% and greater than 75%.

and leftward through the system, since $\bar{\theta}$ at exit is larger, on the average, than $\bar{\theta}$ at entrance. The reversed horizontal temperature gradient above 550 mb appears to be a consequence of latent heat release due principally to mesoscale ascent of saturated air, as we shall see.

f. Water-vapor mixing ratio

The field of mixing ratio is shown in Fig. 11 for Version B. The value drops slowly toward the northwest along the frontal surface, probably because of condensation in the rising air and because of smaller initial values lifted from the surface in the earlier part of the period under study. Overall, the mixing ratio increases slightly from southeast to northwest in the warm air mass up to 650 mb. Above this level it decreases toward the northwest. At all levels there is a relative maximum at some point between +20 and +70 min.

Observed mean relative humidities were between 75 and 85% over much of the region beyond +50 min, where reference to Fig. 4 indicates extensive radar echoes and precipitation at the ground. Since it is difficult to believe that the air was not saturated (or nearly so) in this region, the humidity observations probably suffered a commonly observed low bias. Removal of this bias would increase the analyzed mixing ratio by about 20%, moving the relative maximum to the left in Fig. 11 and perhaps eliminating it altogether at some levels. (The field of $\bar{\theta}_E$ shown in Fig. 9 would also be affected, with maximum increases of about 3 K, which nearly, but not quite, remove the minimum near 600 mb between +40 and +60 min.)

In the flow of air through the system, mixing ratio decreases, principally because of mesoscale ascent of saturated air, with condensation providing the heating discussed above.

5. Apparent sources and sinks of heat and moisture

a. The mesoscale field of motion

An important goal of this investigation is to assess the effect of convection upon the moisture and thermal structure of the next larger scale, in this case, the mesoscale. We will estimate these effects as residuals in budgets in which the transports by the mesoscale motions, as well as the change in storage, are explicitly calculated.

To formalize the approach, we consider the budget for the quantity Q in a mesoscale volume 50 mb deep, 8 km in the y direction, and about 40 km in the x direction. The overbar signifies an average over such a volume. We have

$$\bar{Q}=\frac{\partial\bar{Q}}{\partial t}+\frac{\partial(\bar{u}\bar{Q})}{\partial x}+\frac{\partial}{\partial y}(\bar{v}\bar{Q})+\frac{\partial}{\partial p}(\bar{\omega}\bar{Q})$$
$$+\frac{\partial}{\partial x}(\overline{u'Q'})+\frac{\partial}{\partial y}(\overline{v'Q'})+\frac{\partial}{\partial p}(\overline{\omega'Q'}). \quad (2)$$

Introducing the "apparent" source, we have

$$\dot{Q}^* \equiv \frac{\partial \bar{Q}}{\partial t} + \frac{\partial}{\partial x}(\bar{u}\bar{Q}) + \frac{\partial}{\partial y}(\bar{v}\bar{Q}) + \frac{\partial}{\partial p}(\bar{\omega}\bar{Q}), \tag{3}$$

the rate of change following the mesoscale motion. Then (2) becomes

$$\bar{Q} = Q^* + \frac{\partial}{\partial x}(\overline{u'Q'}) + \frac{\partial}{\partial y}(\overline{v'Q'}) + \frac{\partial}{\partial p}(\overline{\omega'Q'}). \tag{4}$$

We will assume that processes are moist or dry adiabatic, as appropriate, and that the horizontal eddy fluxes are negligible in comparison with the vertical ones. (Estimates in our case indicated that they were an order of magnitude smaller.) We will explicitly calculate $\dot{Q}^*$ from our analyses of the mesoscale mean fields. We will denote $-\partial(\overline{\omega'Q'})/\partial p$ a "virtual" source as $\dot{Q}^V$ (as distinct from that of "real" source, $\bar{\dot{Q}}$) and rewrite (4) as

$$\dot{Q}^* = \bar{\dot{Q}} + \dot{Q}^V. \tag{5}$$

The fields of $\dot{Q}^*$ can be visualized to a good degree of approximation in our case by defining a streamfunction ψ, such that

$$\bar{\omega}_A \equiv \frac{\partial \psi}{\partial y}, \quad \bar{v} \equiv -\frac{\partial \psi}{\partial p},$$

where the approximate vertical motion $\bar{\omega}_A$ is given by

$$\bar{\omega}_A = \bar{\omega}_s + \int_p^{p_s} \frac{\partial \bar{v}}{\partial y} dp.$$

The field of ψ (from Version A of the analyses) has been superposed on the fields of $\bar{\theta}_E$, $\bar{\theta}$ and $\bar{r}$ in Figs. 9, 10 and 11. The Version B field of ψ differs only slightly.

b. *Equivalent-potential temperature*

Under our assumption of adiabatic processes, $\dot{\theta}_E \equiv 0$, so that $\dot{\theta}_E^* = \dot{\theta}_E^V$, i.e., the apparent source is entirely due to the virtual source, presumably associated with convection. Examination of Fig. 9 reveals a pattern which is physically realistic, for the most part. Below 600 mb and prior to the arrival of the SWS, the relatively weak convection is providing a substantial apparent source aloft, by transferring upward the high θ_E values near the ground. The inferred loss in the lower troposphere is being made up in part by residual transfer of heat and moisture from the surface in the last hours of daylight, although there are difficulties in this view, as we shall see.

In the region of vigorous mesoscale ascent and heavy precipitation, convection in the warm air above the frontal surface is effecting a transfer of $\bar{\theta}_E$ from below to above the level of minimum at about 650 mb. The region of apparent loss of $\bar{\theta}_E$ southeast of the SWS and above 550 mb does not lend itself readily to physical explanation and is probably spurious. A relatively small alteration of the fields of meridional component and of $\bar{\theta}_E$ could eliminate much of this apparent loss. Comparison of individual soundings, in fact, suggests no strong divergence aloft southeast of the SWS. Thus, descent which is responsible for the spurious source is largely a consequence of the averaging process.

The apparent rates of change of $\bar{\theta}_E$ are shown quantitatively in Fig. 12., for both versions of the analyses. All terms in (3) were evaluated and the y derivatives were corrected for the time bias discussed earlier. In either version it is evident that changes on the order of 0.1 K min^{-1} are occurring over much of the system. The Version A and Version B patterns are quite similar, the peak values being somewhat smaller in the latter.

c. *Potential temperature*

Examination of the streamfunction pattern in Fig. 10 shows that substantial amounts of apparent heating and cooling are taking place. Just prior to +20 min and in the layer between 700 and 550 mb there is an apparent sink of $\bar{\theta}$ and source of $\bar{\theta}_E$ (Fig. 12). Evidently, rapid evaporation was occurring from tops of short-lived cumulus clouds, consistent with surface observations and nearly total lack of radar echoes in this region. The reality of the cooling above 550 mb is in doubt, as mentioned above.

The large area of apparent heating occurs almost entirely where the mesoscale vertical motion is upward and the air is saturated (or nearly so) on the mesoscale. Thus, it is very difficult to separate the real source, $\bar{\dot{\theta}}$, and the virtual source, $\dot{\theta}^V$, so as to assess the importance of cumulus convection. We are inclined to the view that the convection plays a less important role here than to the southeast, since there is intense apparent heating in the layer from 600 to 650 mb where the virtual source of $\bar{\theta}_E$ is small (Fig. 12). The effect of convection is probably to elevate the level of maximum apparent heating.

The quantitative fields of $\dot{\theta}^*$, for both Versions A and B of the analyses, are shown in Fig. 13. The patterns resemble each other strongly, the latter showing slightly less intense heating. Apparent changes of 0.1°C *per minute* or more cover large areas with peak values reaching 0.5°C *per minute*. For reasons discussed earlier, the center of apparent cooling is probably lower and slightly less intense than shown. The relatively weak cooling (still at the rate of 0.1°C min^{-1}, however) between 600 and 700 mb at the left-hand edge of the figure is probably due to evaporation of precipitation falling from a thick layer of cloud overhead, since the apparent source of $\bar{\theta}_E$ is nearly zero and the mesoscale pattern of relative humidity shows a local minimum in this region.

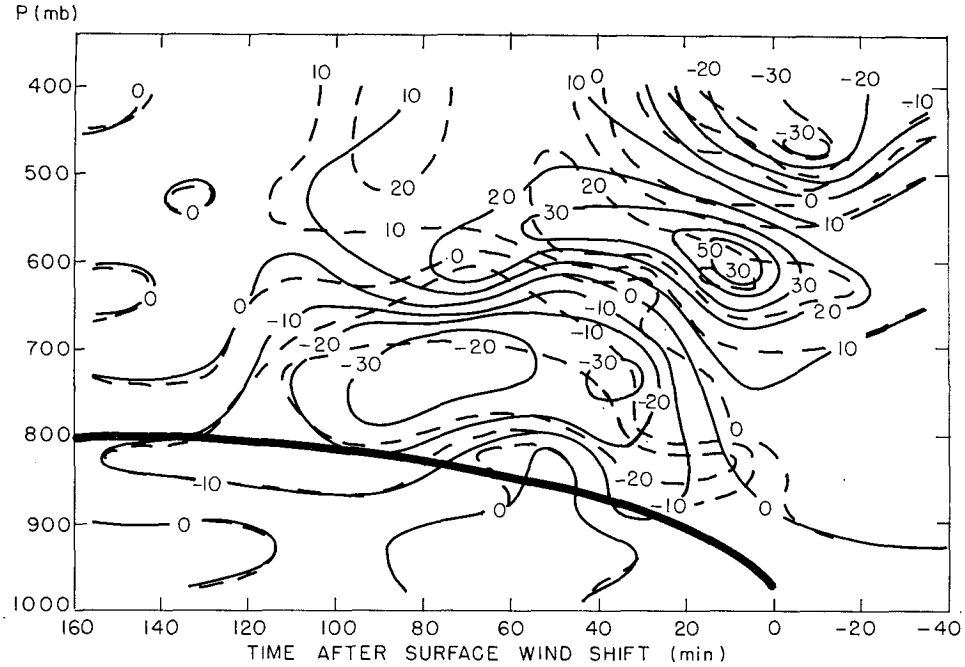

FIG. 12. Apparent source of equivalent potential temperature, $\dot{\theta}_E^*$, labelled in hundredths of degrees K per minute. Solid and dashed lines are for Versions A and B of the analysis, respectively.

d. Water-vapor mixing ratio

The mesoscale flow pattern is superposed on the field of mixing ratio in Fig. 11, and the quantitative field of apparent source appears in Fig. 14. In both Versions A and B there is a region of intense apparent source near 600 mb above the SWS, where we believe that the initial deep cumulus convective clouds set off by the frontal lifting were evaporating into the dry air aloft. Rough estimates indicate that to provide the peak values of cooling and moistening, each cubic

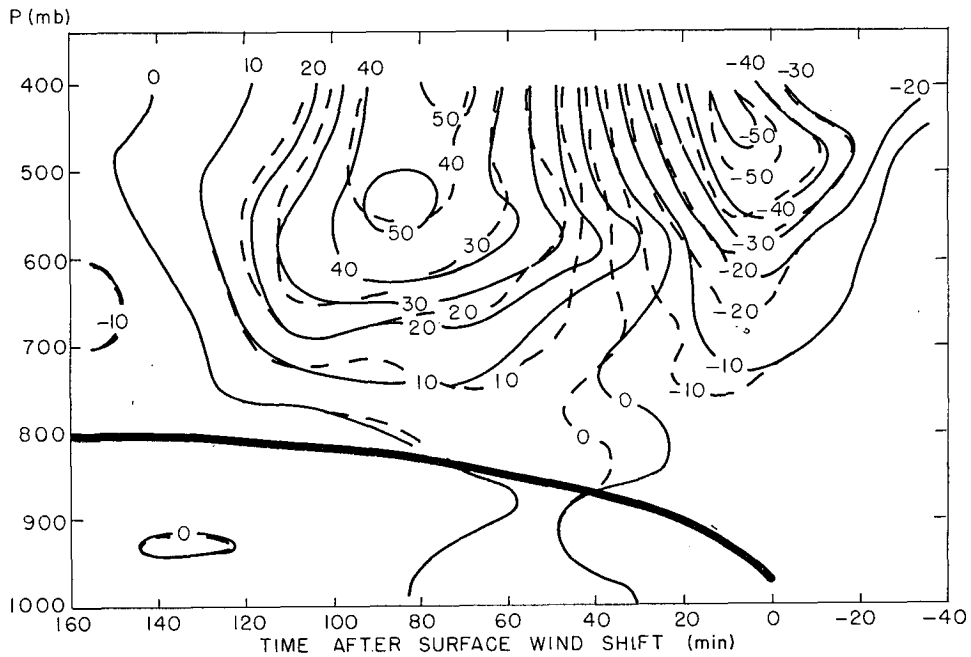

FIG. 13. As in Fig. 12 except for potential temperature, $\dot{\theta}^*$.

meter of cumulus cloud near its top would have to deliver 1 g of liquid water *per minute* for evaporation.

A broader but slightly less intense region of apparent water-vapor loss extends upward and northwestward above the frontal surface. As discussed in the preceding section, this loss represents for the most part condensation in mesoscale ascent of saturated air. The effect of the superimposed convection is to lower the elevation of most intense loss. The weak sources in the shallow cold air and at the left edge of the diagram represent evaporation of precipitation.

In the lower portion of Fig. 14 we show the integrals between 900 and 400 mb of the apparent water-vapor source from -40 to $+40$ min (taking only positive values into account), and of the sink from $+20$ to $+120$ min (taking account only of negative values). The average rainfall rate observed at the 44 surface stations of the network is also shown. All quantities are expressed as equivalent depths of water per 20 min.

Two problems are immediately evident. First, the integrated apparent source plus the precipitation is somewhat larger than the integrated apparent sink. We might attempt to account for the discrepancy in a number of ways. Evaporation from the earth's surface could hardly exceed a few hundreths of a centimeter per 20 min and thus would be negligible. Liquid water would be entering the area in cumulus clouds in the lower right-hand boundary of Fig. 11 but would also be leaving in the form of stratiform cloud in the upper left-hand corner of the diagram. The net accumulation is not likely to be important. The most likely source of error seems to be in the water-vapor transports at the boundaries, but we have argued that the relative humidity aloft at the left boundary suffers a low bias. Thus, if we consider the rainfall measurements as correct, the vapor influx at the right boundary must be too small. The measured relative humidity is probably too low in this region. Such an error is likely during daylight in this region of scattered cloud (Teweles, 1970). Lewis *et al.* (1974) found similar discrepancies in their analysis of a highly similar lower-tropospheric region.

The second difficulty arises at the location of the SWS, where the apparent source aloft (almost certainly a virtual source, since the air is unsaturated on the mesoscale) is evidently not balanced by a virtual sink below as one would expect in the presence of convection. An upward modification of the mixing ratio at low levels near -40 min, as suggested above, would alleviate this problem but probably not solve it.

In all, we share the widespread perception that humidity is the most poorly measured of the common meteorological quantities.

6. Vertical eddy fluxes as measured by balloons

Despite reservations about the use of vertical motions inferred from balloon ascent rates, we undertook to

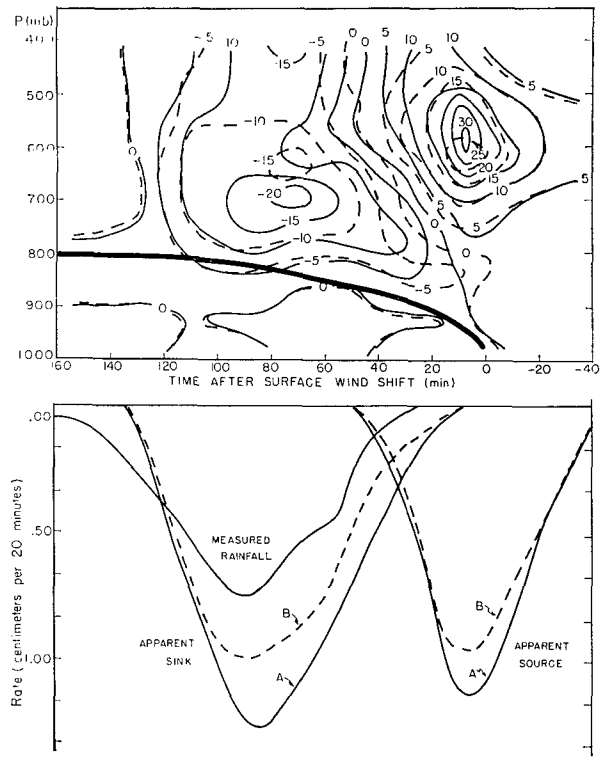

FIG. 14. Upper portion: apparent source of mixing ratio $\dot{r}^*$, labelled in units of 10^{-6} per minute. Solid and dashed lines are as in Fig. 12. Lower portion: measured rainfall and integrated apparent source and sink of mixing ratio. See text.

estimate the virtual source of equivalent potential temperature by obtaining $-\partial(\overline{\omega'\theta_E'})/\partial p$ from the individual balloon soundings comprising the groups of approximately ten which were used in the mesoscale analyses. All balloon measurements were accepted at face value, with no assumptions as to the proportion of volume covered by updrafts.

Results, which appear in Fig. 15, may be compared with the apparent change of $\bar{\theta}_E$ in Fig. 12. The agreement is surprisingly good, with major sources and sinks of similar magnitude and similarly, though not identically, placed. On the whole the virtual source from the balloon data is more intense than the apparent source, probably because the balloons tended to sample the updrafts with an unrepresentatively higher frequency. (It can be shown that with a given difference between updraft and environment $\overline{\omega'\theta_E'}$ has a maximum value when the updraft coverage is 50%.) A major discrepancy occurs near 450 mb above the SWS, where we believe that the apparent sink is incorrect. The source-sink couplet near $+120$ min does not seem credible because it would imply convective transfer through a relatively stable frontal zone (c.f. Fig. 9), and because it is not confirmed in the apparent changes. The agreement between the virtual source and the Version B apparent source near 450 mb at $+90$ min is probably fortuitous,

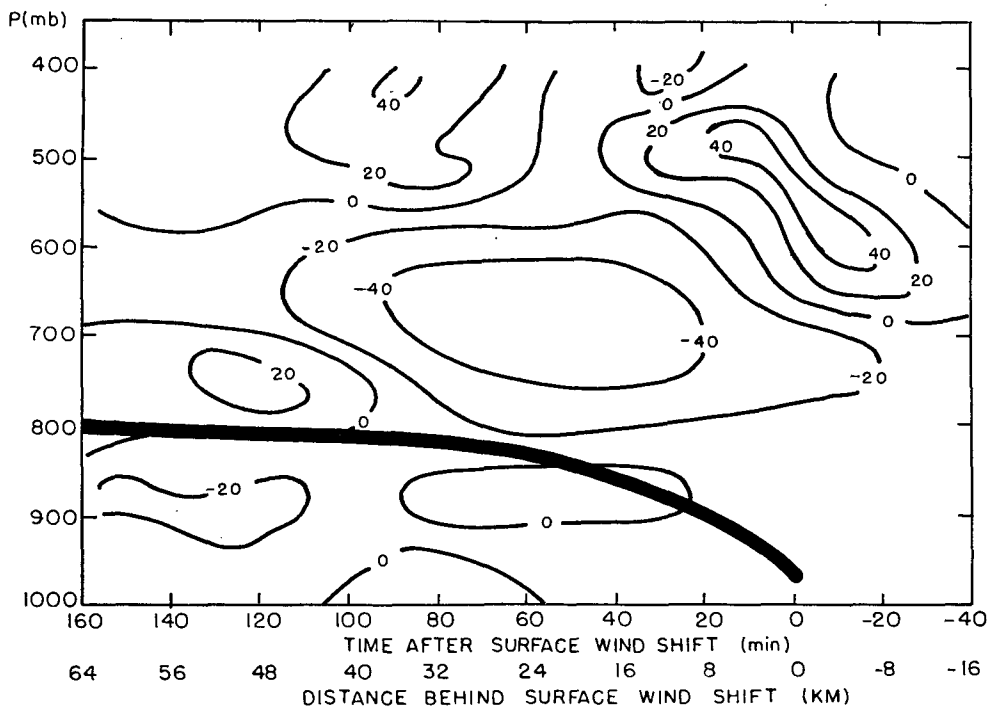

FIG. 15. Virtual source of equivalent potential temperature, $-\partial(\overline{\omega'\theta_E'})/\partial p$, labelled in hundredths of degrees K per minute, as estimated from individual balloon measurements. See text.

since the vertical motion inferred from the balloon ascent rate is particularly doubtful here, as discussed earlier.

It appears, then, that measurements from individual balloons may yield useful information on eddy fluxes in intense convective situations, provided one can make appropriate allowance for their tendency to drift into updrafts.

7. Cumulus convection as simulated by a plume model

Since one of the goals of this study was to see how convection responds to modification of the environment by both the mesoscale motions and the convection itself, we computed a hypothetical cloud at 10 min intervals, using both Version A (however inappropriate) and Version B distributions of temperature and humidity. The model, for a steady-state entraining plume, was taken directly from unpublished MIT class notes of Prof. Norman Phillips. It closely resembles the one proposed by Squires and Turner (1962), from which it does not differ in any physically important way. Computed tops for the Version B environment, for four generous choices of cloud-base radius and updraft speed, are shown for our analysis area in Fig. 16, along with a representative cross section of the NSSL radar observation along 325°, normal to the SWS.

Surface observations in Oklahoma 1–3 h prior to the SWS showed scattered to broken clouds, some of them characterized as towering cumulus but none as cumulonimbus. During the hour immediately preceding the SWS, however, none of the three stations in the Oklahoma City area referred to towering cumulus. The computed tops shown in Fig. 16 seem high in this region, perhaps because of excessive upward mass flux assumed at cloud base.

From surface observations of the location of thunder and lightning relative to the station, it appears that cumulonimbus initially occurred during the first hour after the SWS throughout central Oklahoma. Balloon updrafts were most numerous and intense here as well, and the appearance of intense radar echoes toward the end of the period supports the notion. The computed tops seem realistic here.

Observe, however, that the model tops drop dramatically in the region of maximum radar echo, mesoscale updraft, and observed rainfall, because the water load in the model cloud overcomes the weaker thermal bouyancy, even in a moist environment. Beyond +120 min model clouds will not grow at all, while, paradoxically, thunder was heard from overcast clouds in the Oklahoma City area for at least *five hours* after the SWS. After the time of the radar echo shown in Fig. 16, the pattern became more widespread and less discretely cellular. Observed rainfall at the surface behaved similarly.

We consider that, though the model may have shortcomings, these results support the idea that

thermal bouyancy, in the traditional sense of the term, had little to do with the mesoscale updraft in the region from +60 to +120 min. The situation was clearly not one in which convection, as portrayed by the model, tells us much about what was going on.

8. Concluding discussion

We have analyzed exhaustively a well-documented case of a convectively active cold front in the region of the NSSL meso-network.

In summary, it appears that the purely frontal updraft, up to 0.5 m s^{-1}, first triggers extensive deep convection in a potentially unstable warm air mass as the system passes through the network. An extraordinary response ensues. In the warm air aloft an intense mesoscale downdraft-updraft doublet develops, with the downdraft above the surface wind-shift line and the updraft centered about 30 km to the northwest, toward the colder air. Peak speeds in both of these currents reach about 3 m s^{-1} at the 400 mb level, the downdraft being somewhat narrower and more intense. The vertical currents appear to be driven by a corresponding doublet of cooling and heating with peak rates almost 0.5°C per minute, the former produced by evaporation of the initial deep convective cloud tops in the dry air aloft, the latter by moist-adiabatic ascent on the mesoscale in air of nearly neutral static stability, with superposed convection playing a secondary role. The updraft is further fed by a weak downdraft about 30 km farther to the northwest, due to cooling from evaporation of thundery precipitation falling from a thick "anvil" layer of stratiform cloud streaming northwestward from the updraft.

The potential-temperature field is little perturbed by the mesoscale vertical motions. If it were, it can be argued that ensuing changes of the pressure field would produce accelerations opposed to the existing motion, leading to an oscillatory phenemenon resem-

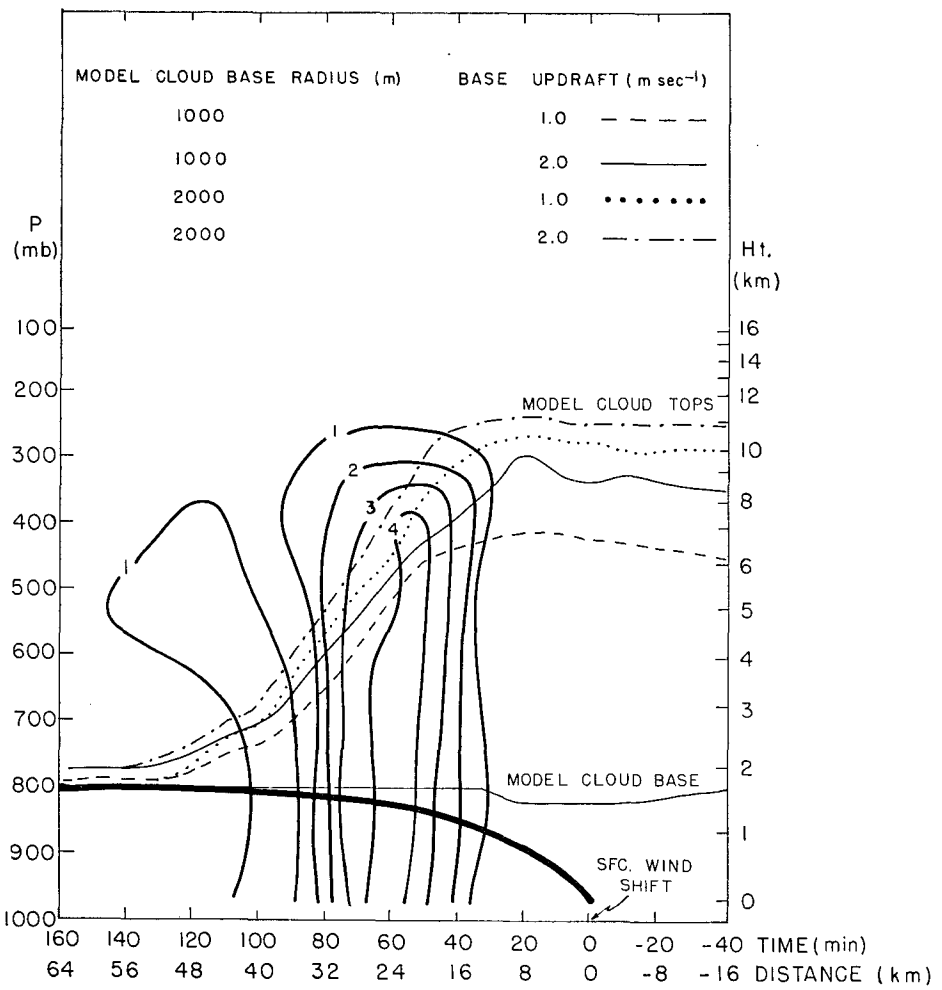

FIG. 16. Base and tops of computed convective plumes, for various combinations of radius and updraft speed at base. Heavy solid lines are contours of radar reflectivity, labelled in units of log Z_e, at 1940 CST along azimuth 325°.

bling a gravity wave. The heating-cooling doublet provides the special circumstances that keep the isentropic surfaces from being distorted and thus permit the mesoscale circulation to be maintained in a nearly steady state for several hours.

Though the storm would be conventionally regarded as convective in character, and though convective phenomena were abundant and intense, the physical essence of the storm seems to resemble an intense elevated sea-breeze circulation rather than a circulation produced by a massive bouyant plume or bubble, or even by a series of them. Brown (1974) has inadvertently produced a numerical result that resembles this case in some important respects, though his model was specialized for the tropics. Convection plays an important, though secondary, role, particularly in providing the needed liquid water for evaporation aloft over the surface wind-shift line.

We appreciate that we have observed a system at maturity and are unable to say much about the physics of its life history that is not purely conjectural. We note that this case did not develop a mesoscale downdraft of convective origin reaching the ground, a feature thought to be characteristic of large thunderstorms (Byers, 1951). We wonder to what extent other severe convective systems resemble this one, noting the crucial importance of evaporation into the dry air aloft and recalling that extremely dry air in the middle troposphere was one of the crucial synoptic ingredients specified by Fawbush *et al.* (1951) for development of tornadic storms. We plan to examine other cases documented in the NSSL archives with these questions in mind.

Acknowledgments. We wish to express our appreciation to Dr. Stanley L. Barnes of NSSL for recommending this case for our consideration, and to Dr. Edwin Kessler, Director of NSSL, for his encouragement and cooperation throughout the long period of study. The authors are indebted also to David I. Katz and Robert Norton of MIT for their assistance in preparation and analysis of data. This work was supported by the National Science Foundation under Grants A36107 and DES 74-24405, and by the National Oceanic and Atmospheric Administration Environmental Research Laboratories under Grant 04-3-022-26.

APPENDIX

Balloon Ascent Rate in Still Air

In a steady-state ascent, the drag (D) and free lift (L) in mass units can be related by

$$D=Lg, \tag{A1}$$

where D can be written as

$$D=\rho\frac{w^2}{2}\frac{\pi d^2}{4}C_d. \tag{A2}$$

In (A2), ρ is air density, w vertical velocity, d sphere diameter, and C_d the drag coefficient. Dimensional analysis shows (Air Ministry Meteorological Office, 1961) that

$$C_d=C\,\mathrm{Re}^n, \tag{A3}$$

where

$$\mathrm{Re}=\frac{w\rho d}{\mu} \tag{A4}$$

is the Reynold's number, μ the coefficient of viscosity, and C and n are pure numbers to be found by experiment.

The total lift of the balloon, $L+M$ (free lift plus mass of load and balloon), can be written as

$$L+M=\pi d^3\rho(1-r)/6, \tag{A5}$$

where r is the density ratio of helium to air at the same pressure and temperature.

Since L, M, d, μ, C, n and ρ are measureable, w as a function of pressure can be found from (A1) through (A5).

If C_d is constant [$m=0$ in (A3)], then w can be expressed as

$$w=w_0\left(\frac{\rho_0}{\rho}\right)^{1/6}, \tag{A6}$$

where the subscript refers to ground values. In this study, d_0 is about 2 m and w_0 is about 6 m s^{-1} (Barnes *et al.*, 1971), so Re at the ground can be determined. Experimental data (MacCready and Jex, 1964) has been used to compute a C_d vs Re relationship for the range of Reynold's numbers that the rising balloons experienced. The effects of cloud turbulence and the low mass of the balloon relative to that of the air were taken into account in arriving at the relationship.

The resulting still-air ascent rate is

$$w=w_0\left(\frac{\rho_0}{\rho}\right)^{0.249}, \tag{A7}$$

which provides for an increase in w from 6.0 m s^{-1} at the ground to 7.1 m s^{-1} at 400 mb. This calculation compares well with prefrontal measurements of an increase in w from 6.0 to 6.9 m s^{-1} at 400 mb, and with experimental values presented by MacCready (1965).

REFERENCES

Air Ministry Meteorological Office, 1961: *Handbook of Meteorological Instruments*, Part II. London, Her Majesty's Stationery Office, 209 pp.

Arakawa, A., and W. Schubert, 1974: Interaction of a cumulus cloud ensemble with the large-scale environment, Part I. *J. Atmos. Sci.*, **31**, 674–701.

Barnes, S. L., J. H. Henderson and R. J. Ketchum, 1971: Rawinsonde observation and processing techniques at the National Severe Storms Laboratory. NOAA TM ERL NSSL-53.

Brown, J. M., 1974: Mesoscale motions induced by cumulus convection: a numerical study. Ph.D. thesis, Massachusetts Institute of Technology.

Byers, H. R., 1951: Thunderstorms. *Compendium of Meteorology*, Thomas Malone, Ed., Amer. Meteor. Soc., 681–693.

Cho, H.-R., and Y. Ogura, 1974: A relationship between cloud activity and the low-level convergence as observed in Reed-Recker's composite easterly waves. *J. Atmos. Sci.*, **31**, 2058–2065.

Fankhauser, J. C., 1969: Convective processes resolved by a mesoscale rawinsonde network. *J. Appl. Meteor.*, **8**, 778–798.

Fawbush, E. J., R. C. Miller and L. G. Starrett, 1951: An empirical method of forecasting tornado development. *Bull. Amer. Meteor. Soc.*, **32**, 1–9.

Lewis, J. M., Y. Ogura and L. Gidel, 1974: Large-scale influences upon the generation of a mesoscale disturbance. *Mon. Wea. Rev.*, **102**, 545–560.

MacCready, P. B., 1965: Comparison of some balloon techniques. *J. Appl. Meteor.*, **4**, 504–508.

——, and H. R. Jex, 1964: Study of sphere motion and balloon wind sensors. NASA TM X-53089, 40 pp.

Ninomiya, K., 1971: Dynamical analysis of outflow from tornado-producing thunderstorms as revealed by ATS III pictures. *J. Appl. Meteor.*, **10**, 778–798.

Ogura, Y., and H. -R. Cho, 1973: Diagnostic determination of cumulus cloud populations from observed large-scale variables. *J. Atmos. Sci.*, **30**, 1276–1286.

Paine, R. J., 1975: A mesoscale study of frontal airflow, moisture and cumulus convection. S.M. thesis, Dept. of Meteorology, Massachusetts Institute of Technology.

Squires, P., and J. S. Turner, 1962: An entraining jet model for cumulonimbus updraughts. *Tellus*, **14**, 422–434.

Teweles, S., 1970: A spurious diurnal variation in radiosonde humidity records. *Bull. Amer. Meteor. Soc.*, **51**, 836–840.

Wonnacott, T. H., and R. J. Wonnacott, 1972: *Introductory Statistics*, 2nd ed. Wiley, 510 pp.

Yanai M., S. Esbensen and J. Chu, 1973: Determination of average bulk properties of tropical cloud clusters from large-scale heat and moisture budgets. *J. Atmos. Sci.*, **30**, 611–627.